Supporting Information

Locally Saturated Ether-Based Electrolytes With Oxidative Stability For Li Metal Batteries Based on Li Rich Cathodes

John Holoubek[1=], Haodong Liu[1=], Qizhang Yan[1=], Zhaohui Wu[1], Bao Qiu[2], Minghao Zhang[1], Sicen Yu[1], Shen Wang[1], Jianbin Zhou[1], Tod A. Pascal[1], Jian Luo[1], Zhaoping Liu[2], Ying Shirley Meng[1], Ping Liu[1]*

[1] Department of NanoEngineering, University of California San Diego, 9500 Gilman Drive, La Jolla, CA, 92093, USA

[2] Ningbo Institute of Materials Technology and Engineering (NIMTE), Chinese Academy of Sciences, Zhejiang, 315201, China

[=] These authors contributed equally

Corresponding authors: piliu@eng.ucsd.edu (P. Liu)

Experimental Methods

Materials

Anhydrous 1,2-dimethoxyethane (DME) were purchased from Gotion and used as received. Bis(2,2,2-trifuloroethyl) ether (BTFE) was purchased from Synquest, and dried with activated molecular sieves for at least 24 hrs before use. Lithium bis(fluorosulfonyl)imide (LiFSI) was obtained from Gotion and used as received. The electrolytes were prepared dissolving predetermined amounts of LiFSI salt into the solvents of interested and stirred. $Li_{1.143}Ni_{0.136}Co_{0.136}Mn_{0.544}O_2$ (LMR) cathode powder was synthesized in the method demonstrated by Guo *et al*.[1] The LMR electrodes were prepared by mixing the NMC 811 powder, Super-P and PVDF (KYNAR 2800) in a ratio of 90:5:5 in N-methyl pyrrolidinone (NMP, Sigma) solvent, cast on Al foil (MTI), dried in a vacuum oven at 120 °C overnight, and calendared in a mechanical roller. For half cell testing, the cathode loading was controlled to ~ 2.8 mAh cm^{-2}, whereas the full cells employed a cathode loading of ~ 4.0 mAh cm^{-2}.

For electrochemical tests CR-2032 or CR-2016 type coin cells were assembled with prepared cathodes and anode separated by a 25 μm Celgard 2325 membrane soaked with 75 μL of electrolyte. For Li metal performance tests, 250 μm Li metal chips were purchased and paired with Cu foil for Li||Cu cells used in Li metal Coulombic efficiency tests, or Al foil in Li||Al cells used in linear scan voltamettry (LSV) tests. LMR half cells were assembled with a 250 μm Li chip vs. the LMR cathode (2.8 mAh cm^{-2}), with aluminum foil protection on the cathode side of the coin

cell case, which has been shown to reduce oxidative reactivity of ether electrolytes.[2] 2x Li||LMR full cells were assembled with an LMR cathode (~4 mAh cm^{-2}) and a limited Li counter electrode that was electroplated beforehand in a separate Li||Cu cell utilizing the LDME 2 electrolyte at an assumed plating efficiency of 96 %. The full cells were finally assembled in CR-2016 coin cells.

Electrochemical Testing

All electrochemical data provided in this work were produced by CR-2032 and CR-2016 type coin cells assembled in an Ar filled glovebox kept at < 0.5 ppm O_2 and < 0.1 ppm H_2O. Cells were rested for at least 4 hr before cycling to allow for complete wetting. Galvanostatic testing was done on Landt CT3001A and Neware BTS 4000 systems. All potentiostatic tests were carried out on a Biologic VSP-300 potentiostat.

Li metal coulombic efficiency (CE) measurements were carried out on Li||Cu cells which consisted of repeated plating (0.5 mA cm^{-2}, 1 mAh cm^{-2}) and stripping (0.5 mA cm^{-2}, 1 V cutoff) cycles. LSV tests were conducted on Li||Al cells scanned to 6.0 V at 5 mV s^{-1} scan rate.

Li||LMR cells were assembled and subjected to galvanostatic cycling from 2-4.6 V, regardless of loading or N/P ratio. Room temperature cycling consisted of 3 conditioning cycles at C/10 followed by C/3 indefinitely for half cells, and C/3 for 50 cycles followed by 3 more cycles at C/10 for full cells. The specific capacity basis for C rate determination was 275 mAh g^{-1} with respect to the cathode.

Characterization

XPS (Kratos Analytical, Kratos AXIS Supra) was carried out using Al anode source at 15 kV and all the peaks were fitted based on the reference C-C bond at 284.6 eV. All XPS measurements were collected under a 300 mm × 700 mm spot size. Survey scans were collected with a 1.0 eV step size, and were followed by high resolution scans with a step size of 0.05 eV for C 1s, O 1s, F 1s, and S2p regions. XPS samples were obtained from LMR half cells applying excess Li counter electrodes after 1 and 100 cycles in the noted electrolyte, which were then disassembled, washed with DME, and allowed to dry before beind placed in a heat-sealed bag inside the glovebox before they were transferred to the XPS.

The morphology of the deposited Li metal at various temperatures was characterized using a FEI Quanta 250 SEM. The samples were obtained from coin cells and rinsed briefly with DME before analysis. All prepared samples were placed in an aluminum-laminated heat-sealed bag inside the glovebox before they were transferred to the SEM.

TEM characterization of the CEI was conducted using a JEOL 2800 TEM at 200 kV. STEM-EDX experiment was conducted using a JEOL JEM-ARM300CF at 300 kV. For CEI characterization, Gatan 626 single tilt cooling holder was used to decrease the sample temperature to about -170 ^{o}C to minimize TEM beam damage on CEI morphology. TEM characterization of the surface cation mixing layer was conducted in a separate session using a

double-tilt holder at room temperature. The cycled electrode crystal structure was shown to be stable under electron beam at room temperature. To prepare the TEM sample, the cathode powder was gently scraped off from the electrode inside an Ar-filled glovebox. The powder was then collected with a Cu grid and sealed using an aluminum laminated pouch bag. During TEM sample loading, direct Ar flow was maintained toward the sample holder to minimize air exposure.

Molecular Dynamics Simulations

Molecular Dynamics (MD) simulations were performed in LAMMPS, with the solvent and Li^+ described by the OPLS-AA forcefield[3] and FSI^- described by Gaouveia et al.[4] MD simulation boxes containing ~250 total molecules were constructed using the provided mol ratios of each system. In all cases the charges of the Li^+ and FSI^- molecules were scaled to the high-frequency dielectric properties of the solvents present in the system according to the method demonstrated by Park *et al*.[5] These scaling values were 0.73, 0.75, 0.76, and 0.76, 1 M LiFSI in DME, LDME 1, LDME 2, and LDME 3, respectively.

For each system, an initial energy minimization at 0 K with energy and force tolerances of 10^{-4} was performed to obtain the ground-state structure. After this, the system was heated from 0 K to 298 K at constant volume over 0.01 ns using a Langevin thermostat, with a damping parameter of 100 ps. The system was then subjected to 5 cycles of quench-annealing dynamics in order to eliminate the persistence of any meta-stable states, where the temperature was slowly cycled between 298 K and 894 with a ramp period 0.025 ns followed by 0.1 ns of dynamics at either temperature extreme. After annealing, the system was equilibrated in the constant temperature (298 K), constant pressure (1bar) (NpT ensemble) for 1.0 ns followed by 0.5 ns of constant volume (NvT ensemble) dynamics. We resolved stresses in the system isotropically using the Andersen barostat (pressure relaxation constant of 1 ps). We used the Shinoda et al.[6] equations of motion, combining the hydrostatic equations of Martyna et al.[7] and the strain energy proposed by Parrinello and Rahman[8]. Finally, we performed 25 ns of constant volume, constant temperature (NVT) production dynamics at 298 K.

Radial distribution functions were obtained using the Visual Molecular Dynamics (VMD) software. Solvation speciation was determined via a series of in-house scripts. First, each Li^+ and every molecule within 3 Å were sampled every 0.1 ns via a Tcl script implemented through VMD, which generated thousands of structure files per run. Next, the number of DME, FSI^-, and BTFE in each snapshot were tallied using Python and aggregated into a distribution of $Li(DME)_x(FSI)_y(BTFE)_z^{y+1}$ complexes.

Cell-Level Energy Density and Raw Material Cost Projection

The cell-level energy density projections shown in Figure 1 were calculated using a model based on pouch-type full cells composed of multiple layers of 4.4 x 5.7 cm cathodes and 4.5 x 5.8

cm anodes. For the pouch cell film, we assume a 2 mm allowance on each side of the electrodes for sealing purposes with the total film length defined by the stack thickness. The thicknesses and densities for the current collectors, separators, binder, and conductive carbon were all taken from Betz *et al*.[9] The pouch cell electrode tabs and laminated film characteristiccs were measured experimentally from materials purchased from MTI. Cathode powder tap densities were taken from commercial powders sold from MTI, and LMR cathode tap density was assumed to be comparable to NMC powders, at 2.3 g cm^{-3}. The achievable specific capacities for LFP, NMC 111, NMC 811, and LMR were assumed to be 155, 155, 200, and 260 mAh g^{-1}, respectively. The average discharge voltages for LFP, NMC 111, NMC 811, and LMR were assumed to be 3.2, 3.8, 3.8, and 3.55 V, respectively. The active cathode active mass fraction was assumed to be 96 %, with 2 % conductive carbon and 2 % PVDF binder. The cathode porosity was set at 30 % in all cases. The Li metal anode (3860 mAh g^{-1}) was set at 2x excess capacity (N/P = 2) relative to the cathode, with a porosity of 0 %. In all cases, the electrolyte loading was set to 3 g Ah^{-1}, a loading that has already been achieved and surpassed by Li metal pouches in the literature.[10,11] In all cases, an electrode stacking scheme with X double-layer anodes, X-1 double-layer cathodes, and 2 single-layer cathodes was employed, and X was adjusted at a given cathode loading to achieve a total cell capacity as close as possible to 5 Ah. Raw material costs were obtained on *tradingeconomics.com* in January 2023, and weighed based on the given stoichiometric ratio between components of each cathode material.

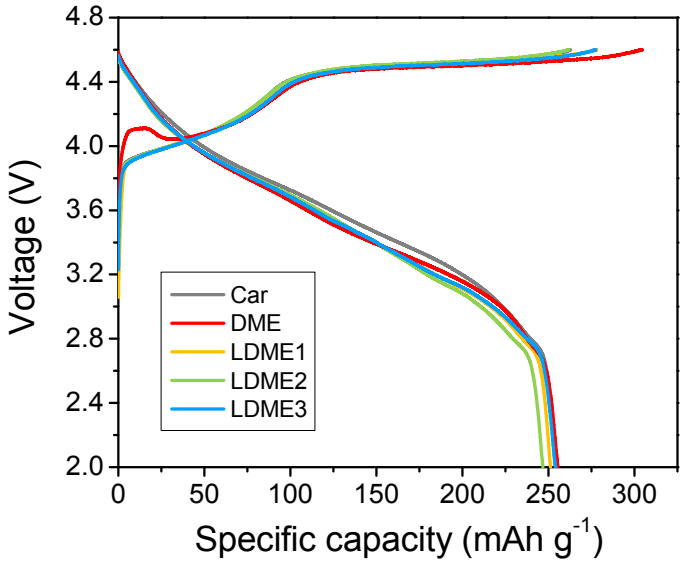

Figure S1. 1st cycle voltage curves of LMR half cells applying electrolytes of interest.

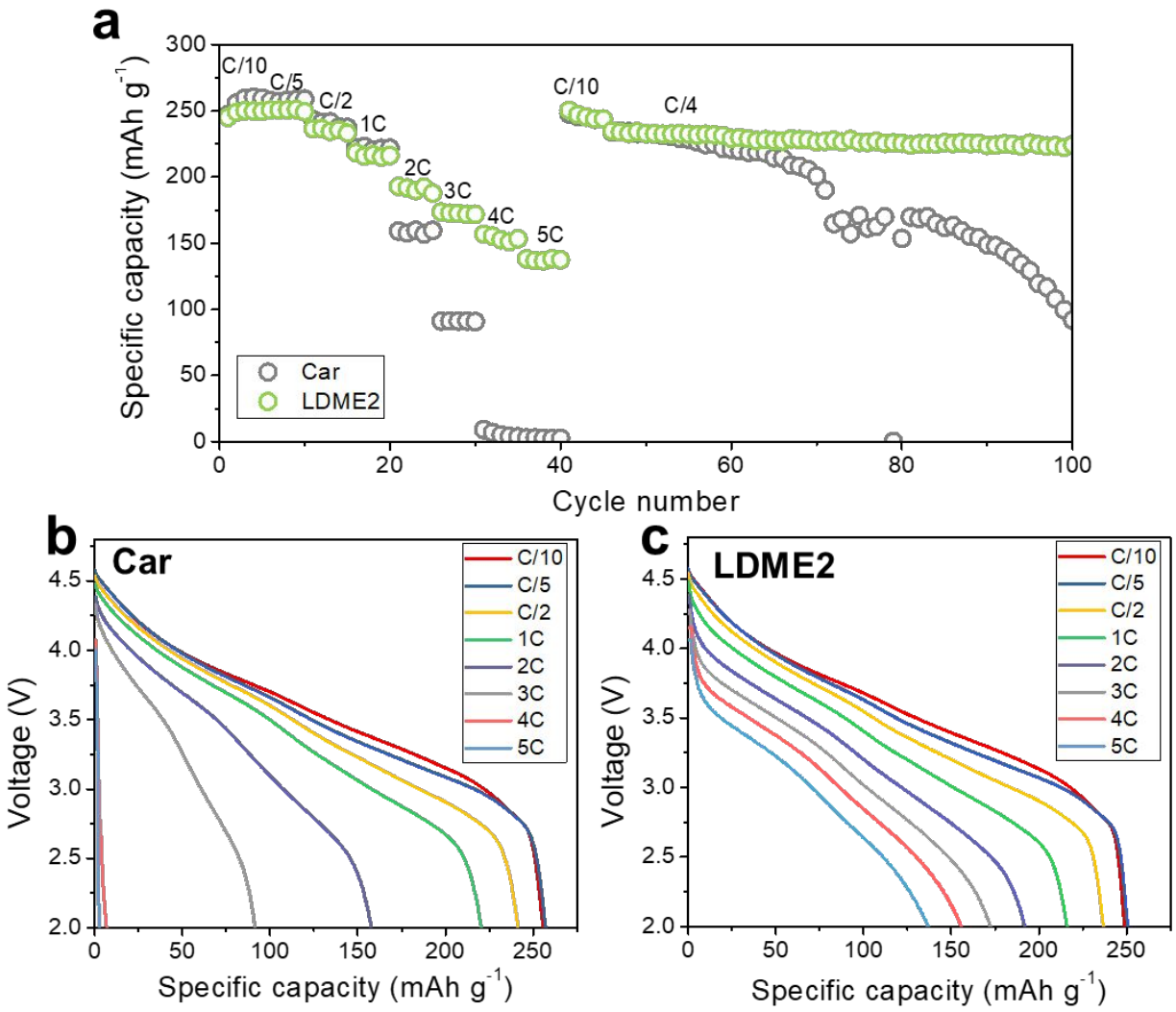

Figure S2. Discharge rate performance of LMR half cells in LDME2 and carbonate electrolytes. **a)** Variable discharge rate cycling performance when after charging at C/10. Associated discharge profiles in **b)** carbonate and **c)** LDME2 electrolytes.

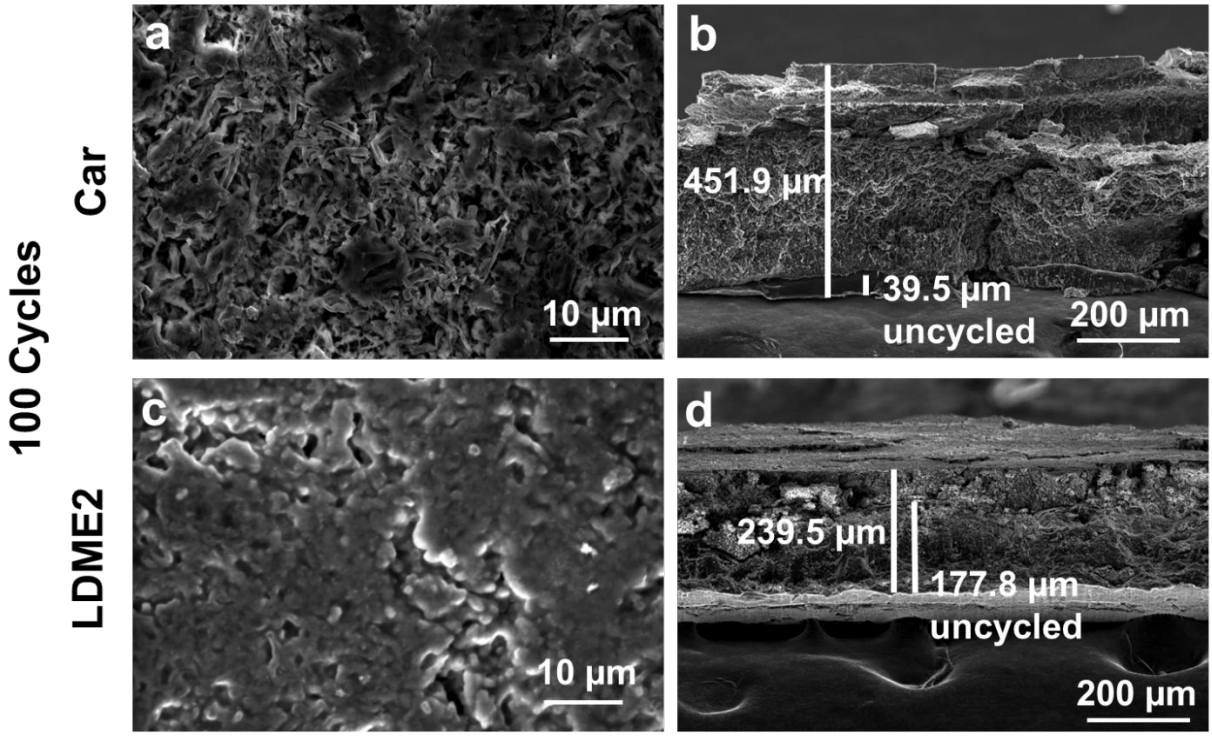

Figure S3. Scanning electron microscopy of Li counter electrodes after 100 cycles in half cells. Morphology of Li cycled in the carbonate electrolyte from **a)** top and **b)** cross-sectional views. Morphology of Li cycled in the LDME2 electrolyte from **c)** top and **d)** cross-sectional views.

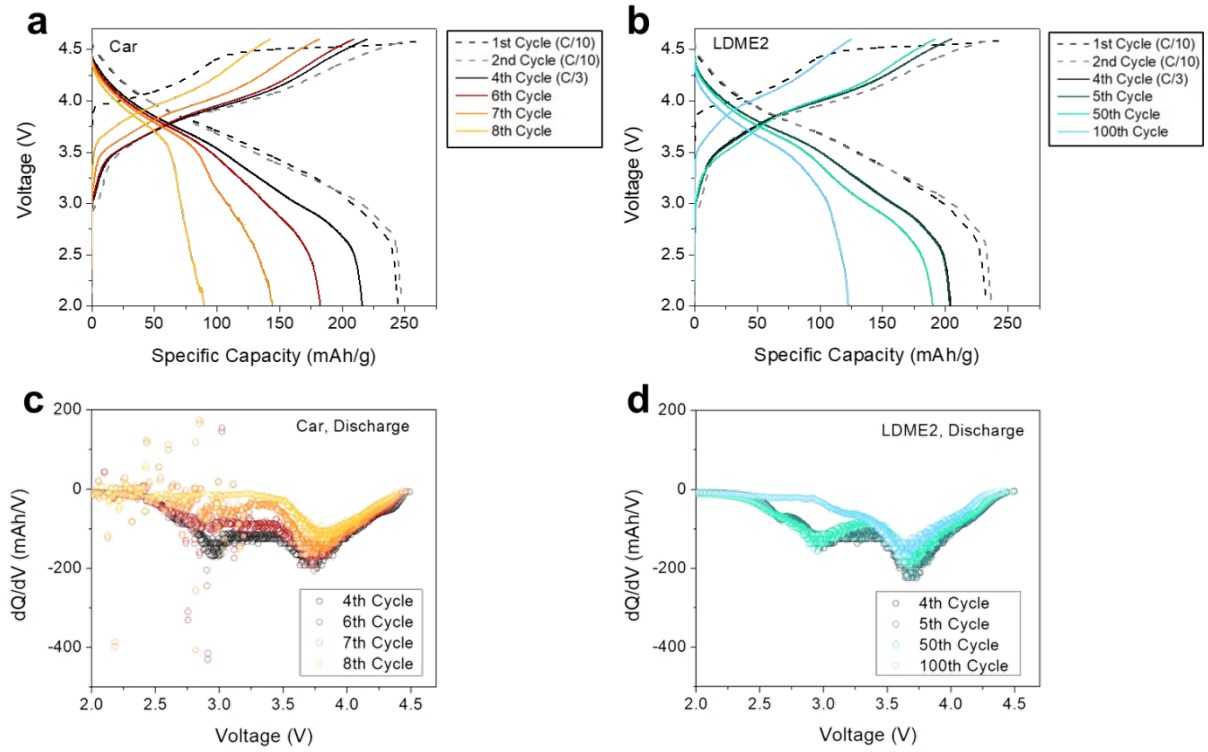

Figure S4. Additional electrochemical data of full cells shown in Figure 4d. Voltage curves from cells applying **a)** Carbonate and **b)** LDME2 electrolytes. Corresponding dQ dV^{-1} discharge curves from cells applying **c)** Carbonate and **d)** LDME2 electrolytes.

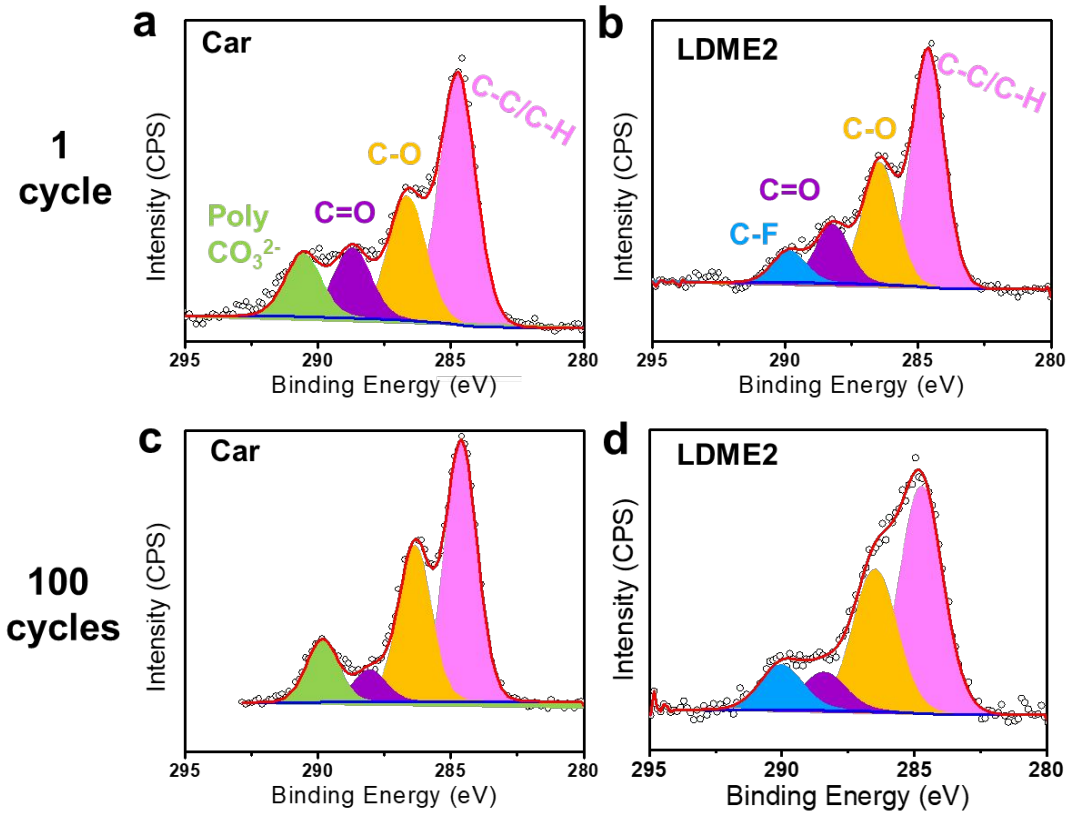

Figure S5. XPS C1s spectra of Li counter electrodes after 1 cycle in **a)** carbonate and **b)** LDME2 electrolytes. C1s spectra of Li counter electrodes after 100 cycle in **c)** carbonate and **d)** LDME2 electrolytes.

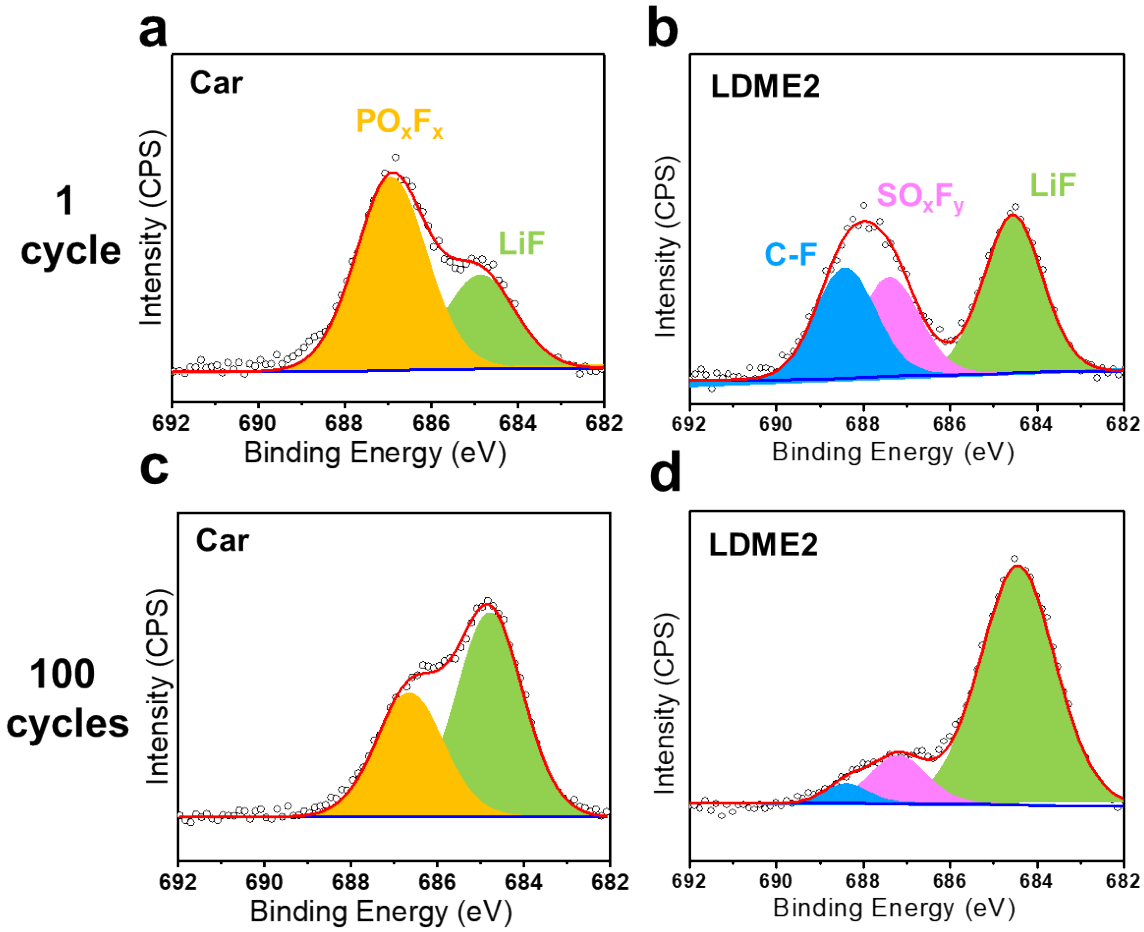

Figure S6. XPS F1s spectra of Li counter electrodes after 1 cycle in **a)** carbonate and **b)** LDME2 electrolytes. F1s spectra of Li counter electrodes after 100 cycle in **c)** carbonate and **d)** LDME2 electrolytes.

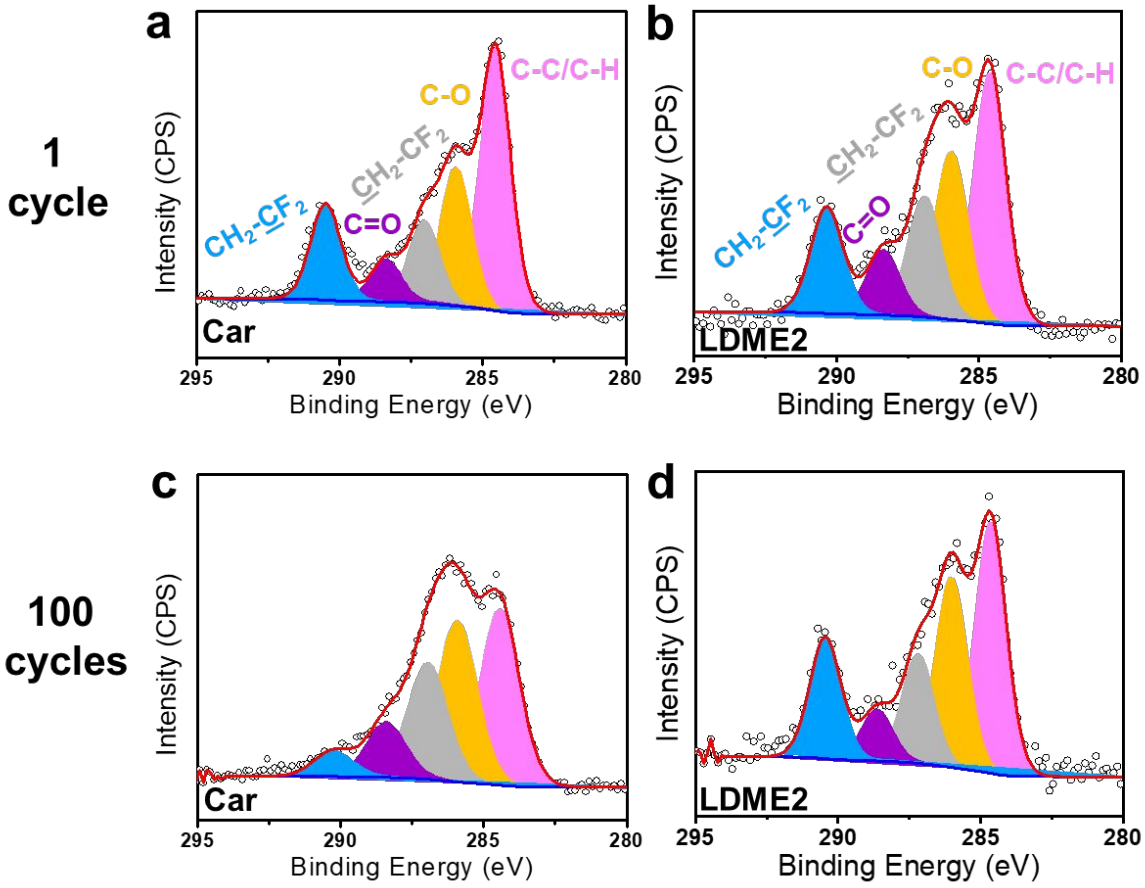

Figure S7. XPS C1s spectra of LMR cathodes taken from half cells after 1 cycle in **a)** carbonate and **b)** LDME2 electrolytes. C1s spectra of LMR cathodes after 100 cycles in half cells using **c)** carbonate and **d)** LDME2 electrolytes.

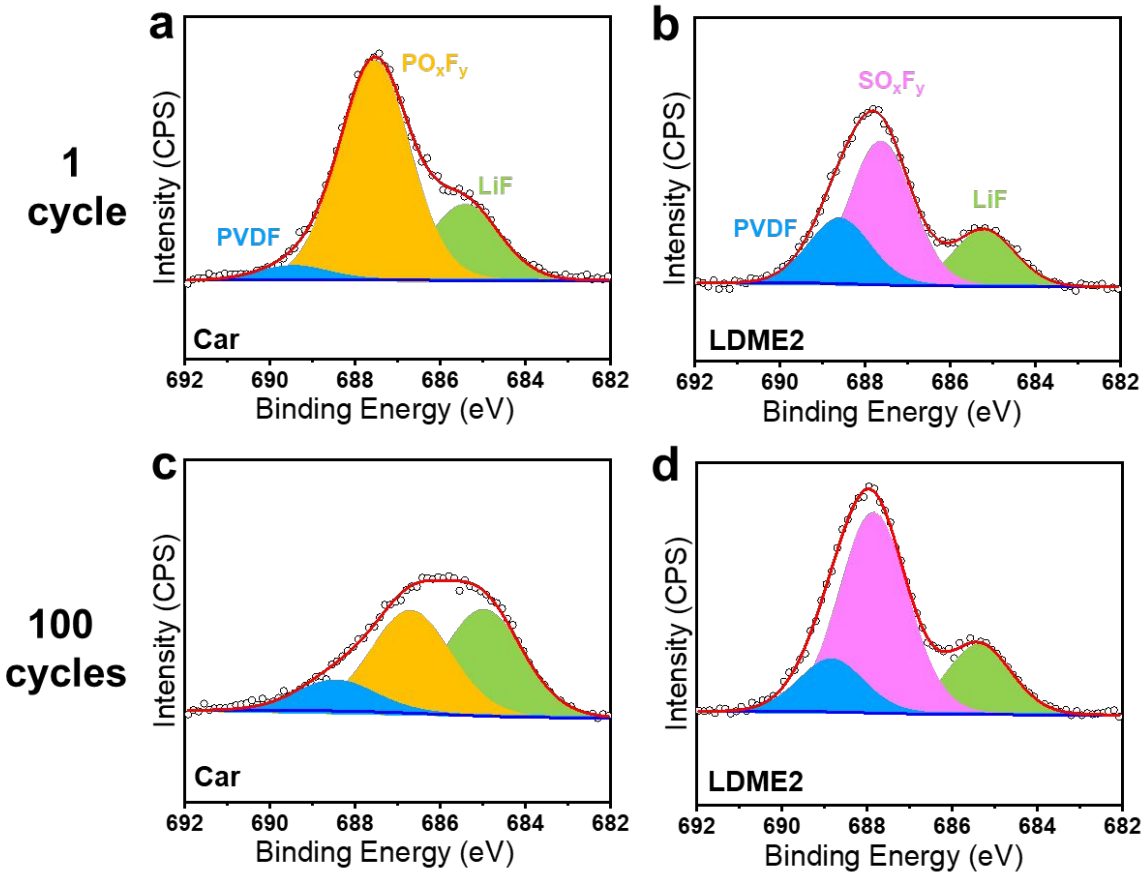

Figure S8. XPS F1s spectra of LMR cathodes taken from half cells after 1 cycle in **a)** carbonate and **b)** LDME2 electrolytes. F1s spectra of LMR cathodes after 100 cycles in half cells using **c)** carbonate and **d)** LDME2 electrolytes.

References

(1) Guo, H.; Jia, K.; Han, S.; Zhao, H.; Qiu, B.; Xia, Y.; Liu, Z. Ultrafast Heterogeneous Nucleation Enables a Hierarchical Surface Configuration of Lithium-Rich Layered Oxide Cathode Material for Enhanced Electrochemical Performances. *Advanced Materials Interfaces* **2018**, *5* (11), 1701465.

(2) Ren, X.; Zou, L.; Cao, X.; Engelhard, M. H.; Liu, W.; Burton, S. D.; Lee, H.; Niu, C.; Matthews, B. E.; Zhu, Z.; Wang, C.; Arey, B. W.; Xiao, J.; Liu, J.; Zhang, J.-G.; Xu, W. Enabling High-Voltage Lithium-Metal Batteries under Practical Conditions. *Joule* **2019**, *3* (7), 1662–1676.

(3) Kaminski, G. A.; Friesner, R. A.; Tirado-Rives, J.; Jorgensen, W. L. Evaluation and Reparametrization of the OPLS-AA Force Field for Proteins via Comparison with Accurate Quantum Chemical Calculations on Peptides. *J. Phys. Chem. B* **2001**, *105* (28), 6474–6487.

(4) L. Gouveia, A. S.; S. Bernardes, C. E.; C. Tomé, L.; I. Lozinskaya, E.; S. Vygodskii, Y.; S. Shaplov, A.; Canongia Lopes, J. N.; M. Marrucho, I. Ionic Liquids with Anions Based on Fluorosulfonyl Derivatives: From Asymmetrical Substitutions to a Consistent Force Field Model. *Physical Chemistry Chemical Physics* **2017**, *19* (43), 29617–29624.

(5) Park, C.; Kanduč, M.; Chudoba, R.; Ronneburg, A.; Risse, S.; Ballauff, M.; Dzubiella, J. Molecular Simulations of Electrolyte Structure and Dynamics in Lithium–Sulfur Battery Solvents. *Journal of Power Sources* **2018**, *373*, 70–78.

(6) W. Shinoda, M. Shiga, M. Mikami, Rapid estimation of elastic constants by molecular dynamics simulation under constant stress, Physical Review B 69 (2004) 134103.

(7) G.J. Martyna, D.J. Tobias, M.L. Klein, Constant pressure molecular dynamics algorithms, J. Chem. Phys. 101 (1994) 4177-4189.

(8) M. Parrinello, A. Rahman, Polymorphic transitions in single crystals: A new molecular dynamics method, J. Appl. Phys. 52 (1981) 7182-7190.

(9) Betz, J.; Bieker, G.; Meister, P.; Placke, T.; Winter, M.; Schmuch, R. Theoretical versus Practical Energy: A Plea for More Transparency in the Energy Calculation of Different Rechargeable Battery Systems. *Advanced Energy Materials* **2019**, *9* (6), 1803170.

(10) Niu, C.; Lee, H.; Chen, S.; Li, Q.; Du, J.; Xu, W.; Zhang, J.-G.; Whittingham, M. S.; Xiao, J.; Liu, J. High-Energy Lithium Metal Pouch Cells with Limited Anode Swelling and Long Stable Cycles. *Nature Energy* **2019**, *4* (7), 551–559.

(11) Niu, C.; Liu, D.; Lochala, J. A.; Anderson, C. S.; Cao, X.; Gross, M. E.; Xu, W.; Zhang, J.-G.; Whittingham, M. S.; Xiao, J.; Liu, J. Balancing Interfacial Reactions to Achieve Long Cycle Life in High-Energy Lithium Metal Batteries. *Nature Energy* **2021**, *6* (7), 723–732.